Line tension approaching a first-order wetting transition: Experimental results from contact angle measurements

J. Y. Wang, S. Betelu,* and B. M. Law
Condensed Matter Laboratory, Department of Physics, Kansas State University, Manhattan, Kansas 66506
(Received 2 June 2000; published 21 February 2001)

The line tension values of *n*-octane and 1-octene on a hexadecyltrichlorosilane coated silicon wafer, are determined by contact angle measurements at temperatures near a first-order wetting transition T_w. It is shown experimentally that the line tension changes sign as the temperature increases toward T_w in agreement with a number of theoretical predictions. A simple phenomenological model possessing a repulsive barrier at $l_0 = 5.1 \pm 0.2$ nm and a scale factor of $B = 78 \pm 6$ provides a quantitative description of the experiments.

DOI: 10.1103/PhysRevE.63.031601 PACS number(s): 68.08.Bc, 68.03.Cd, 68.35.Md

I. INTRODUCTION

During the past few decades the line tension, which is the excess energy associated with the contact line at the boundary between three bulk phases, has attracted the attention of numerous theoretical [1–14] and experimental [15–33] research groups. Although this thermodynamic quantity was proposed over 100 years ago by Gibbs [34], the magnitude and even the sign of the line tension are still not understood experimentally within an acceptable margin [35]. This is unfortunate because the line tension plays an extremely important role in determining the contact angle for microscopic droplets [27,35], the nucleation behavior of droplets on surfaces [36–38], the dynamics of contact line spreading [39,40], the attachment of solid particles to a fluid interface [41], and the formation of Newton black films and foam films [42–45].

Theoretical analysis of the excess energy in the region of the three-phase contact line indicates that the magnitude of the line tension is very small: of order 10^{-12} to 10^{-10} N [5–14]. However, experiments have determined line tension values ranging from 10^{-12} to 10^{-5} N, where some measurements [26–33] are 5–6 orders of magnitude larger than any theoretical estimation of the line tension. Such a large variation in the magnitude of the experimental line tension may arise from nonequilibrium conditions within the system [45,46]. There are many difficulties associated with accurately determining the line tension experimentally because its magnitude is believed to be small. For example, to determine the correct line tension from contact angle versus droplet size data (see details below) for a droplet situated on a solid surface the basic requirements are (i) an accurate contact angle technique, (ii) a molecularly smooth and homogeneous solid surface, and (iii) a highly purified liquid. The presence of any surface-active liquid contaminants or solid surface imperfections, heterogeneities, and/or roughness are believed to significantly influence the magnitude of the line tension.

In the theoretical analysis the line tension τ is predicted to be related to the interaction potential $V(l)$, where $l = l(x)$ represents the thickness of the liquid film as a function of position x in the vicinity of the boundary [Eq. (11) below]. Early experiments never investigated the close connection between τ and $V(l)$. An appropriate way of studying this interrelationship is to measure τ in the vicinity of a phase transition, such as a first-order wetting transition where the potential $V(l)$ is known to change markedly as a function of temperature; hence τ is expected also to vary dramatically with temperature. There are extensive theoretical predictions for the variation of τ in the vicinity of a wetting transition [47–65]; however, only recently has our group completed an experimental study of τ in the vicinity of a first-order wetting transition [66] which could be compared with theory.

The aim of this publication is to provide more complete experimental details concerning our line tension measurements in the vicinity of a first-order wetting transition. This paper is organized as follows. In Sec. II we briefly review the theoretical considerations for the behavior of the line tension near a first-order wetting transition. In Sec. III we describe the procedures used in preparing a molecularly smooth and homogeneous solid surface. The microscopic interferometer used in measuring the line tension is also described in this section. The experimental results are presented and discussed using a simple phenomenological model in Sec. IV. The paper concludes with a summary in Sec. V. A number of auxiliary considerations related to the interpretation of the interferometric image of the droplet are confined to an Appendix.

II. THEORY

A. Young's equation and the line tension

Consider a simple three-phase system, such as a droplet resting on a *perfect* homogeneous, horizontal, isotropic solid surface. If this droplet is sufficiently large so that the effects of the three-phase contact line can be neglected, the change of the free energy due to the change in droplet size can be written as

$$\begin{aligned} dF &= \sigma_{sl} dA_{sl} + \sigma_{sv} dA_{sv} + \sigma_{lv} dA_{lv} \\ &= (\sigma_{sl} - \sigma_{sv} + \sigma_{lv} \cos\theta_\infty) dA_{sl}, \end{aligned} \tag{1}$$

where F is the free energy, A is the area of an interface where the subscripts s, l, v correspond, respectively, to the *solid*, *liquid*, and *vapor* phases, σ is the surface free energy or surface tension, and θ_∞ is the contact angle of the droplet.

*Present address: School of Mathematics, University of Minnesota, Minneapolis, MN 55455.

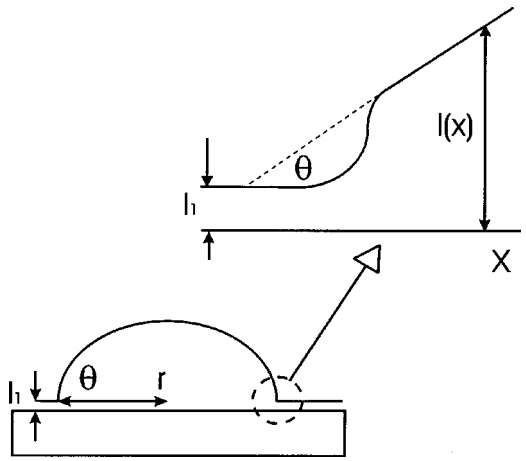

FIG. 1. Schematic diagram of a microscopic droplet situated on a solid substrate. The droplet has a contact angle θ and base radius r and is in mechanical equilibrium with an adsorbed layer of thickness l_1. The interface displacement profile $l(x)$ is also shown in the vicinity of the solid and/or liquid and/or vapor contact line.

At (mechanical) equilibrium F is a minimum ($dF=0$) and we obtain Young's equation [7,25]

$$\sigma_{sv}=\sigma_{sl}+\sigma_{lv}\cos\theta_\infty, \tag{2}$$

which describes the mechanical equilibrium of the forces (per unit length) on the three-phase contact line in the plane of the solid surface.

Young's equation (2) is strictly valid only for macroscopic droplets at mechanical equilibrium with any adsorbed film of thickness l_1 (Fig. 1) on a molecularly smooth horizontal solid surface. For microscopic droplets the contact angle will be influenced by surface interactions and the nature of the three-phase solid-liquid-vapor contact line of length L_{slv}, which will contribute an additional free energy per unit length or line tension τ to the excess free energy of the droplet. This effect adds an excess energy term τdL_{slv} to Eq. (1) [35]. Hence for a spherical droplet of contact angle θ and lateral radius r (Fig. 1), we obtain the modified Young's equation [2,67]

$$\sigma_{sv}=\sigma_{sl}+\sigma_{lv}\cos\theta+\frac{\tau}{r} \tag{3}$$

which can alternatively be written as

$$\cos\theta=\cos\theta_\infty-\frac{\tau}{r\sigma_{lv}}, \tag{4}$$

where θ_∞ is the contact angle in the limit of very large droplets ($r\to\infty$). Hence from Eq. (4) the quantities τ and $\cos\theta_\infty$ can be determined from a study of $\cos\theta$ as a function of $1/r$.

The contact angle θ_∞ provides important information about the wettability of a surface. A liquid partially wets a surface if a large droplet possesses a finite contact angle, $\theta_\infty>0$. If, however, this liquid has a contact angle $\theta_\infty=0$ the liquid completely wets the surface and the surface is covered by a thick liquid film. For an appropriate solid-liquid combination (as we will see later in this paper) it is sometimes possible to find a wetting transition as a function of increasing temperature where below a wetting temperature T_w a droplet possesses a finite, nonzero contact angle θ_∞ whereas above T_w the contact angle $\theta_\infty=0$.

The wettability of a surface is sometimes expressed in terms of the spreading coefficient [68]

$$S\equiv\sigma_{sv}-(\sigma_{sl}+\sigma_{lv}) \tag{5}$$

which compares the energy of a solid-vapor surface (σ_{sv}) with the energy when this surface is covered by a thick wetting film ($\sigma_{sl}+\sigma_{lv}$). From Eqs. (2) and (5) therefore

$$S=\sigma_{lv}(\cos\theta_\infty-1). \tag{6}$$

Hence for partial wetting, where $T<T_w$ and θ_∞ is nonzero, $S<0$. While for complete wetting, where $T\geqslant T_w$ and $\theta_\infty=0°$, $S=0$. The singularity in S at T_w can be written as [53]

$$-S\propto(T_w-T)^{2-\alpha_s}, \tag{7}$$

or, equivalently

$$\cos\theta_\infty\propto-(T_w-T)^{2-\alpha_s}, \tag{8}$$

where α_s is the surface specific-heat exponent while σ_{lv} is assumed constant over a small temperature interval. The order of the wetting transition at T_w is determined by the value of the exponent α_s. If $\alpha_s=1$ then dS/dT is discontinuous at T_w and the wetting transition is first order; alternatively, from [Eq. (8)], if $\cos\theta_\infty$ depends linearly upon $\Delta T=T_w-T$ then the wetting transition is first order. For higher-order wetting transitions the slope dS/dT will approach zero continuously at T_w, i.e., $\alpha_s<1$.

B. Line tension approaching a first-order wetting transition

The contact angle decreases and vanishes on raising the temperature to the wetting transition temperature T_w [69]. The line tension is therefore only defined for $T<T_w$; above T_w the three-phase contact line disappears. A number of different theoretical approaches have been used to study the singular behavior of the line tension at T_w. These approaches have produced vastly different results for τ [47–65] where this quantity was observed to be zero, finite, or diverge to infinity at T_w and so, for a time, there was great confusion concerning the theoretically predicted behavior of the line tension at T_w. A consensus has recently been reached [50–65] which is summarized in [53]. It is found that the singular behavior of the line tension, upon approaching T_w, depends sensitively on both the *order of the wetting transition* and the *range of the intermolecular forces*.

Indekeu used an ''interface displacement model'' to predict the features of the line tension near T_w [50]. This model is a useful tool for studying the behavior of the line tension near wetting. We review Indekeu's model below and use it to interpret our line tension measurements near T_w later. The key point of this model is that the inhomogeneity of the three-phase contact line is described by a single-valued interface displacement profile $l(x)$, where x is a coordinate

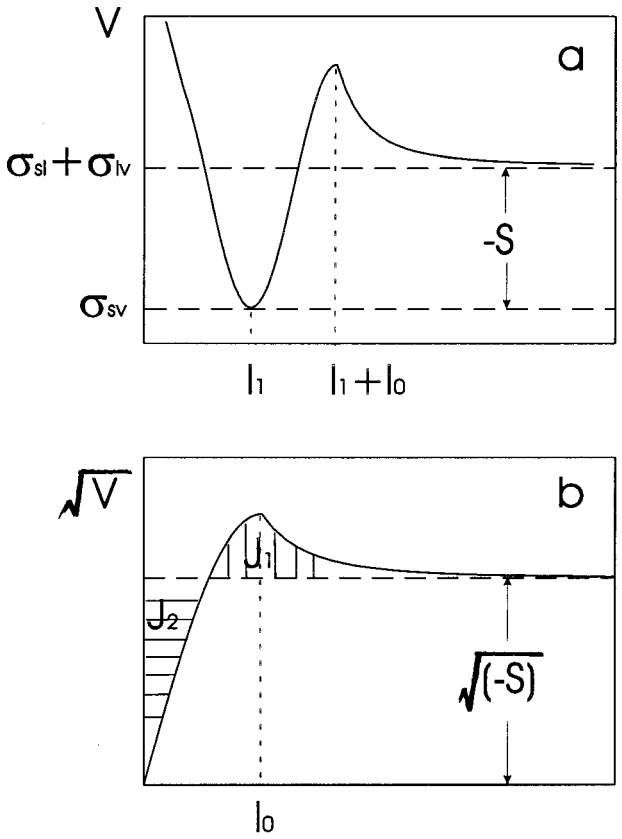

FIG. 2. (a) A typical interface potential $V(l)$ for partial wetting described by Eq. (13) where a repulsive barrier exists at l_1+l_0. The adsorbed film of thickness l_1 has a lower energy σ_{sv} than a thick film or droplet, at $l\to\infty$, with energy $\sigma_{sl}+\sigma_{lv}$. (b) Plot of $\sqrt{V(l)}$ as a function of thickness l for the above potential where the adsorption minimum has been shifted to the origin. The shaded areas J_1 and J_2 of the function $\sqrt{V(l)}$ determine the line tension of a droplet according to Eq. (12).

parallel to the substrate and $l(x)$ is the thickness of the profile at position x. A typical shape for $l(x)$, at partial wetting, is shown in Fig. 1 where the shape varies from a microscopically thin adsorbed film of thickness l_1 to a macroscopically thick droplet of lateral radius r and contact angle θ.

In the interface displacement model the line energy $\Gamma[l(x)]$ is written as a functional of the profile $l(x)$,

$$\Gamma[l(x)]=\int_{-\infty}^{\infty} G(l,l_x)dx+\text{const}, \tag{9}$$

where the integration proceeds from the thin-film state (at $x=-\infty$) to the bulk liquid (at $x=\infty$). The integrand $G(l,l_x)$ is the surface excess free energy, which can be expressed as

$$G(l,l_x)=\frac{1}{2}\sigma_{lv}\left(\frac{dl}{dx}\right)^2+V(l), \tag{10}$$

where the first term is the surface excess free energy cost due to any increase in interfacial area while the second term is the *interface potential* which represents the excess free energy per unit area due to the presence of a uniform film of thickness l. At partial wetting ($T<T_w$) the interface potential $V(l)$ has the typical shape depicted in Fig. 2(a). This potential possesses a *global* energy minimum σ_{sv} at l_1, corresponding to a microscopically thin adsorbed film of thickness l_1, and a *local* energy minimum $\sigma_{sl}+\sigma_{lv}$ at $l\to\infty$, corresponding to the presence of a macroscopically thick droplet on the surface. An energy barrier at l_1+l_0 separates the global minimum from the local minimum where the difference between these two energy minima $V(\infty)-V(l_1)=-S$. For a first-order wetting transition $-S$ [Eq. (7)] and $\cos\theta_\infty$ [Eq. (8)] vary linearly with T on approaching T_w, until at T_w, $S=0$ and the two minima possess precisely the same energy. Above T_w the thin adsorbed film is now a local minimum while the thicker wetting film is a global minimum; hence another signature of a first-order wetting transition is the presence of a thin adsorbed film l_1 which increases *discontinuously* to a large and perhaps macroscopic thickness ($l\to\infty$) at the wetting temperature T_w [70]. A *continuous* increase in the adsorption thickness l_1 with temperature to a large and perhaps macroscopic value could be an indication of the presence of a second-order wetting transition [71].

The equilibrium droplet profile (Fig. 1) corresponds to that function $l(x)$ which possesses the minimum line energy or line tension $\tau=\Gamma[l(x)]|_{\min}$. It can be shown that [50]

$$\tau=B\sqrt{2}\sigma_{lv}l_0\int_0^{\infty}dL[\sqrt{V(L)/\sigma_{lv}}-\sqrt{-S/\sigma_{lv}}] \tag{11}$$

$$=B\sqrt{2\sigma_{lv}}l_0[J_1-J_2], \tag{12}$$

where for convenience the adsorption minimum has been placed at the origin ($l_1=0$) and the integration over the dimensionless thickness $L=l/l_0$ extends from the adsorption minimum out to the infinitely thick droplet. An arbitrary scale factor B has been included in Eq. (11) where the theories [50] assume that $B=1$. Equation (11) can also be expressed via a graphical representation to the shaped areas, J_1 and J_2, depicted in Fig. 2(b) which connects the shape of $[V(l)]^{1/2}$ to τ.

A qualitative understanding of τ can be obtained by examining how Fig. 2(b) varies as a function of temperature in the vicinity of a first-order wetting transition. When $T\ll T_w$ the value of $\sqrt{-S}$ is large and the area J_2 dominates J_1 so that τ is *negative* according to Eq. (12). However, as T approaches T_w the spreading coefficient $S\to 0$ and therefore the area $J_2\to 0$, hence τ is *positive and perhaps infinite* depending upon the area J_1 at T_w. This positivity of τ at T_w is a consequence of the repulsive barrier between the two minima at l_1 and $l=\infty$ in the interface potential $V(l)$. This characteristic feature, for first-order wetting transitions, that the line tension τ changes sign as the temperature approaches T_w is evident in the theoretical calculations of many authors [61–65].

An explicit expression for the interface potential is required before the line tension can be calculated. The following dimensionless potential

$$V(L)/\sigma_{lv}=\begin{cases}A(1)[1-\cos(\pi L)]/2, & 0\leqslant L<1\\ A(L), & L\geqslant 1\end{cases} \tag{13}$$

where $A(L)=W_0/L^2-S/\sigma_{lv}$ and $W_0=W/\sigma_{lv}l_0^2$, will be used in later calculations. It includes many realistic features: it is harmonic ($\sim l^2$) at $l\ll l_0$ with a repulsive barrier at $l\sim l_0$ while for large $l\gg l_0$ it exhibits a nonretarded interaction $V(l)\sim W/l^2-S$ which correctly decays to $-S$ at very large $l\to\infty$ [see Fig. 2(a)]. The spreading coefficient S in this potential is related to θ_∞ [see Eq. (6)] or T (using Fig. 7), while the Hamaker constant W is a system-dependent constant. The *shape* of the potential and the *height* of the repulsive barrier is controlled by the length l_0.

Indekeu [53] also derived explicit expressions for the variation of the line tension with temperature in the vicinity of a first-order wetting transition from Eq. (11) for various interaction potentials. He found that

$$\tau=\tau_0-\tau_1 X, \tag{14}$$

where X takes the form $t^{1/2}\ln(1/t)$ for short-range (SR) interactions [$V(l)\sim e^{-l}$], $\ln t$ for nonretarded long-range (NLR) interactions [$V(l)\sim l^{-2}$], and $t^{1/6}$ for retarded long-range (RLR) interactions [$V(l)\sim l^{-3}$], and the reduced temperature $t\equiv(T_w-T)/T_w, \tau_1>0$ while $\tau_0=\tau(t=0)>0$ for SR and RLR interactions. For each of these situations τ changes from a negative to a positive value with increasing absolute slope $|d\tau/dt|$ as T_w is approached. At T_w τ is positive and finite for SR and RLR interactions while it is infinite for NLR interactions.

III. EXPERIMENTS

The early work of Zisman [72] on the wettability of surfaces provides valuable information which can be used in determining which liquid-solid surface combinations will exhibit a wetting transition as a function of temperature. In these early studies it was found that the wettability of a solid surface could be characterized by the molecular group which was predominant at the interface. For example, Zisman and co-workers prepared a number of surfaces where the methyl group —CH_3 formed the outer most molecular group at the interface by coating a solid surface with a self-assembled monolayer (SAM) possessing this end group. The wettability of this type of interface was characterized by determining the droplet contact angle θ_∞ for a homologous series of organic liquids; a ''Zisman plot'' of $\cos\theta_\infty$ as a function of the surface tension of these liquids defined the critical surface tension σ_c for the surface where $\cos\theta_\infty=1$. Liquids with a surface tension $\sigma>\sigma_c$ formed droplets with a finite contact angle on the surface whereas liquids with a surface tension $\sigma<\sigma_c$ completely wet the surface. A Zisman plot of the *n*-alkanes determined that —CH_3 possessed a critical surface tension $\sigma_c\approx 24$ mN/m. Later work qualitatively confirmed this picture: Wasserman, Tao, and Whitesides [73] found that —CH_3 had a $\sigma_c\approx 24$ mN/m while Brzoska, Ben Azouz, and Rondelez [74] found that σ_c ranged from 20 to 23 mN/m for —CH_3 where the precise value depended rather sensitively upon the length of the SAM and also upon the specific preparation conditions under which the SAM was formed.

For a liquid with $\sigma>\sigma_c$ at room temperature, a wetting transition should occur at sufficiently high temperature provided the liquid does not boil first. This follows from the fact that according to Eq. (6) $S<0$ at room temperature (as $\theta_\infty>0$) while with increasing temperature σ_{lv} is expected to decrease much faster than $\sigma_{sv}-\sigma_{sl}$ because the thermal expansion coefficient of liquids is much larger than the thermal expansion coefficient of solids, hence S should approach zero [Eq. (5)] with increasing temperature. In this study we examine wetting transitions that occur for ''alkane like'' liquids deposited on molecularly flat Si wafers that had been coated with a self-assembled monolayer where the outermost molecular group is a methyl group (—CH_3).

A. Materials

The liquids used in this experiment are *n*-octane [$CH_3(CH_2)_6CH_3$] (99+%) and 1-octene [$CH_3(CH_2)_5CH=CH_2$] (98+%) purchased from Aldrich Chemical Company and used without further purification. The (100) silicon wafers were purchased from Semiconductor Processing Company. The original wafers were polished on one side, possessed *n*-type phosphorus doping with a resistivity of 1–10 Ω cm, thickness 0.3 cm, and radius 7.6 cm. These wafers were subsequently diced into quarters by the company for ease of handling. The surface of the wafer is typically covered by a uniform oxide layer of thickness ~2 nm.

B. Silanization of the Silicon Wafer

The preparation of self-assembled monolayers on the molecularly smooth Si wafer followed a fairly standard procedure [73,74].

(1) The wafers were first covered with a tough plastic adhesive tape to protect the polished surface from dust and scratching. They were then diamond sawed to a size of ~2 cm×2 cm.

(2) The tape was removed and the wafers were rinsed and ultrasonically cleaned in chloroform for 15–20 min to remove any gross organic impurities.

(3) The wafers were then cleaned in a solution of 30% H_2O_2 + 70% H_2SO_4 for 30 min at 120°C which effectively removes any trace organic impurities on the surface. During this time the wafers were continuously shaken in this solution. Following this procedure the wafers were rinsed well in 18 $M\Omega$ cm distilled deionized water and stored in a beaker of this clean water prior to silanization.

(4) After complete drying using a warm jet of air, the wafers were immersed for more than 2 h in a silane solution composed of 70 ml hexadecane, 30 ml carbon tetrachloride, and 0.5 ml of *n-hexadecyl-trichlorosilane* which was maintained at a temperature of 18 °C. This procedure was performed inside a closed, sealed plastic preparation bag, where the humidity was kept below 30% using phosphorus pentoxide (P_2O_5).

(5) The wafers were finally removed, rinsed in chloroform, and shaken for 15 min in an ultrasonic bath of chloroform. After this preparation procedure the wafers were stored immersed in the same liquid to be studied in order to elimi-

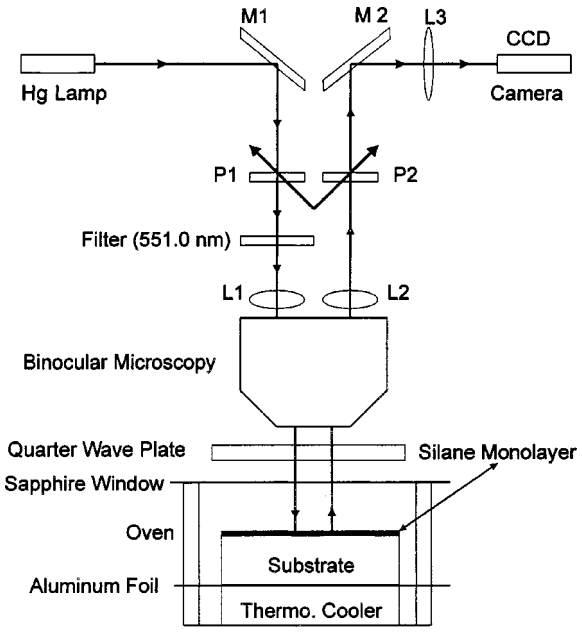

FIG. 3. Schematic diagram depicting the microscopic interferometry technique and sample chamber. M1, M2, reflecting mirrors; P1, P2, crossed polarizers; L1, L2, L3, lenses. The quarter wave plate ensures that only light reflected from the substrate passes through polarizer P2 to the CCD camera.

nate the accumulation of dust particles on the surface.

It is believed that this procedure creates a chemically bonded silane monolayer to the underlying Si wafer. In the experiments below (Sec. IV) we find that this surface possesses a low critical surface tension $\sigma_c \approx 19$ mN/m and low contact angle hysteresis in approximate agreement with previous measurements [74]. An atomic force microscopy (AFM) study of this monolayer confirms the absence of any atomic-sized pinholes in an area $10 \times 10\ \mu m^2$ where the surface roughness ~ 5 Å is characteristic of the underlying surface roughness for a bare silicon wafer.

C. Experimental setup

Previous techniques used for contact angle measurements [24–31] are incapable of studying droplets possessing small contact angles ($<10°$) because of limited accuracy ($0.5°-3°$). Hence the surface transition from partial to complete wetting could not be studied. In this paper we describe a microscopic interferometry technique that can study droplets with contact angles in the range $\sim 2°-10°$ with high accuracy for droplet radii $\sim 1-100\ \mu$m. This technique is therefore ideally suited for studying line tension effects in small droplets in the vicinity of a wetting transition where θ_∞ is small. The optical configuration is schematically shown in Fig. 3. A droplet on the Si wafer substrate is illuminated by the 551 nm mercury line. This light first passes through the linear polarizer P1 and is incident upon a quarter wave plate via one arm of the binocular microscope. The quarter wave plate converts the light to circular polarized light. After reflection from the wafer and/or droplet surface and a second pass through the quarter wave plate, the light is converted to linear polarized light but turned by 90° with respect to the

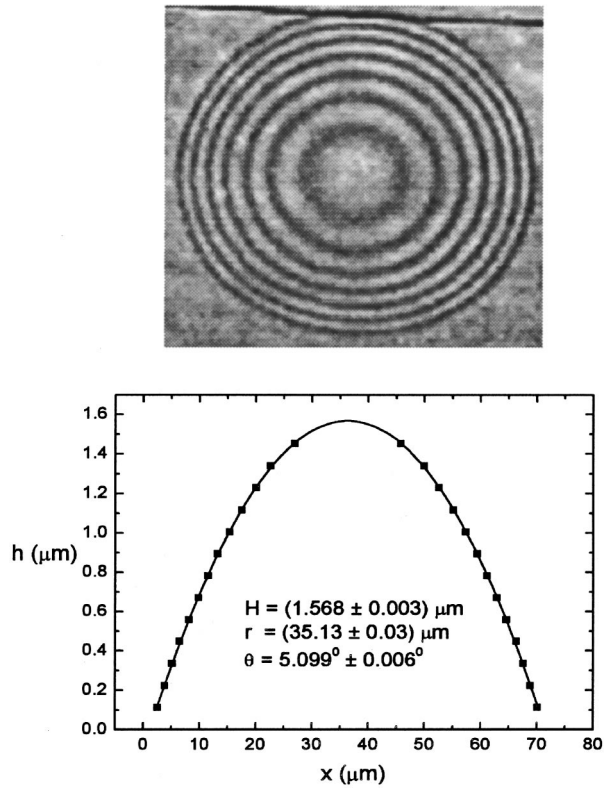

FIG. 4. Droplet image which shows the interference fringes for octane at a temperature of 40.9°C. The constructive and destructive interference fringes (solid squares) are fitted to a spherical cap shaped droplet using Eq. (15) from which the center thickness (H) and base radius (r) of the droplet are determined. The contact angle is then calculated using Eq. (17).

illuminating beam. After propagating through the other arm of the binocular microscope the second polarizer P2 allows this light to be incident upon the charge-coupled device (CCD) camera. Stray light reflected from surfaces within the microscope, and above the quarter wave plate, cannot pass through the crossed polarizer P2. In order to optimize the measurement of the interference pattern within the droplet the binocular microscope was modified as follows. One eye piece was replaced by lens L1 which, together with the microscope objective lens (OL), illuminated the droplet and wafer with plane parallel light. The other eye piece possessed a 100-μm square grid. Lens L2 focused the grid while the combination of L2 and OL focused the droplet and wafer surface to the same image plane. Lens L3 then projected these overlapping images of the grid and droplet onto the CCD camera. Real-time images of a droplet at a specific temperature were recorded and shown on a television screen connected to the CCD camera.

If the substrate surface is smooth and homogeneous, a spherical droplet is formed by vapor deposition on the substrate, and a circular droplet image with interference fringes is observed on the television screen, as shown in Fig. 4. This digitized image is analyzed by a computer program to determine the radius (r_i) of each black (minimum) or bright (maximum) fringe. The spherical cap shape for the droplet is then fitted via a least-squares method to

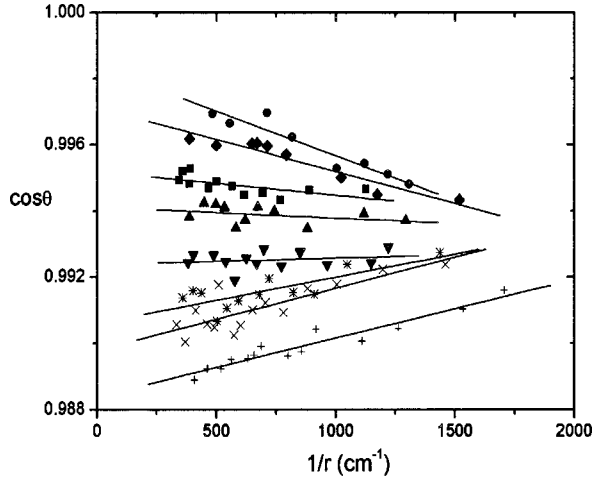

FIG. 5. Plot of $\cos\theta$ versus $1/r$ for droplets of 1-octene on a hexadecyltrichlorosilane coated Si wafer at various temperatures $T=40.7$ (pluses), 42.1, 43.1, 44.0, 46.0, 47.3, 48.6, and 50.0 °C (solid circles). The solid lines are linear fits to the data from which the line tension τ and $\cos\theta_\infty$ can be obtained according to Eq. (4).

$$h_i = H\left[1-\left(\frac{r_i}{r}\right)^2\right] \tag{15}$$

to obtain the center thickness (H) and the base radius (r) of the droplet (Fig. 4). In this equation

$$h_i = i\lambda/2n \quad (i=0,\tfrac{1}{2},1,\tfrac{3}{2},\ldots) \tag{16}$$

is the thickness of the droplet associated with the ith fringe. Half-integral values of i correspond to minima (black fringes) while integral values of i correspond to maxima (bright fringes), $\lambda(=551$ nm) is the wavelength of light, and $n(=1.40)$ is the refractive index of liquid. The contact angle θ is finally determined from

$$\theta = \arctan(2H/r). \tag{17}$$

Least-squares fits to the droplet shape show that the contact angle is obtained to better than $\pm 0.01°$ while the contact line radius r is obtained to better than $\pm 0.1\,\mu$m for big droplets or $\pm 0.01\,\mu$m for small droplets ($r<20\,\mu$m). The accuracy of Eqs. (15) and (16) are discussed in the Appendix.

In studying the line tension near a wetting transition it is important to be able to control the temperature and vary the radius r of the droplet in a continuous fashion [see Eq. (4)]. The sample chamber was designed for this purpose. This chamber was constructed from aluminum in the form of two sections which were separated by a thin aluminum foil (Fig. 3). The upper section, in which the liquid and Si wafer were placed, was wrapped with heating wire and acted as an oven which was controlled by a Lakeshore DRC-91CA temperature controller. A thermoelectric cooler, which was in close contact with the Si wafer, was placed underneath the aluminum foil in the lower chamber. The aluminim foil acted as a clean impenetrable barrier between the thermoelectric cooler and the highly purified liquid and clean Si wafer. Droplets could be grown slowly on the Si wafer by maintaining a small temperature difference between the temperature of the substrate and the temperature of the oven. The top of the chamber was covered by a sapphire window whose c axis was parallel to the beam propagation direction. Droplets on the substrate were readily evaporated by opening this cover window.

TABLE I. The values of τ and θ_∞ at different temperatures for octane.

Temperature T(°C)	Line tension $\tau(10^{-10}$ N)	Contact angle θ_∞(°)
28.0	-4.4 ± 0.8	9.545
29.2	-3.6 ± 1.4	9.305
30.5	-2.9 ± 0.6	8.791
31.8	-4.7 ± 0.9	8.559
33.3	-2.5 ± 0.9	7.844
34.9	-1.9 ± 0.6	7.343
36.7	-0.6 ± 0.6	6.822
38.2	-1.3 ± 0.4	6.202
39.8	-0.2 ± 0.6	5.543
40.9	0.1 ± 0.2	5.020
42.0	1.3 ± 0.5	4.248
43.3	2.4 ± 0.3	2.916

IV. RESULTS AND DISCUSSION

In Fig. 5 we show a plot of $\cos\theta$ versus $1/r$ at various temperatures for an octene droplet vapor-deposited on the silane coated silicon wafer where the solid lines are linear fits to the data. A similar plot was also measured for octane droplets on this surface. From the modified Young's equa-

TABLE II. The values of τ and θ_∞ at different temperatures for octene.

Temperature T(°C)	Line tension $\tau(10^{-10}$ N)	Contact angle θ_∞(°)
40.7	-1.7 ± 0.3	8.735
42.1	-1.8 ± 0.7	8.190
43.1	-1.4 ± 0.7	7.858
44.0	-0.2 ± 0.6	7.078
46.0	0.3 ± 0.6	6.045
47.3	0.7 ± 0.5	5.622
48.6	1.8 ± 0.4	4.357
50.0	2.5 ± 0.6	3.282

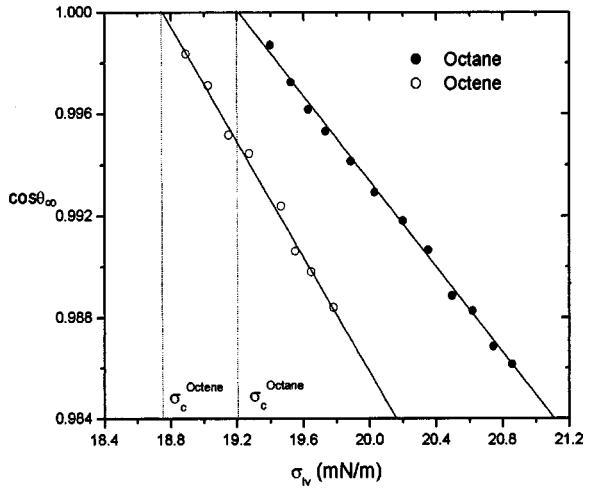

FIG. 6. Plot of $\cos\theta_\infty$ as a function of surface tension σ_{lv} for *n*-octane and 1-octene. The solid lines are linear fits to the data while the critical surface tension σ_c corresponds to $\cos\theta_\infty=1$.

tion (4) the line tension τ and $\cos\theta_\infty$ can be deduced where the surface tension variation $\sigma_{lv}^{\text{Octane}}=23.52-0.09509T$ mN/m and $\sigma_{lv}^{\text{Octene}}=23.68-0.09581T$ mN/m [75] have been used in this deduction. The values for τ and θ_∞ at each temperature are tabulated in Tables I and II for octane and octene, respectively.

As mentioned previously the critical surface tension σ_c is an important quantity for characterizing an interface. In Fig. 6 we show a Zisman plot [72] of $\cos\theta_\infty$ as a function of σ_{lv} for the two liquids. From this plot the critical surface tensions (corresponding to $\cos\theta_\infty=1$) are $\sigma_c^{\text{Octane}}=19.20\pm0.01$ mN/m and $\sigma_c^{\text{Octene}}=18.75\pm0.01$ mN/m. In Fig. 7 we plot $\cos\theta_\infty$ now as a function of T in order to deduce the wetting temperatures $T_w^{\text{Octane}}=(45.4\pm0.1)\,^\circ$C and $T_w^{\text{Octene}}=(51.2\pm0.1)\,^\circ$C (corresponding to $\cos\theta_\infty=1$). The linear relationship of $\cos\theta_\infty$ with T exhibited in Fig. 7 indicates that the wetting transition in this experiment is indeed first order. We note that the wetting transition temperature T_w is very

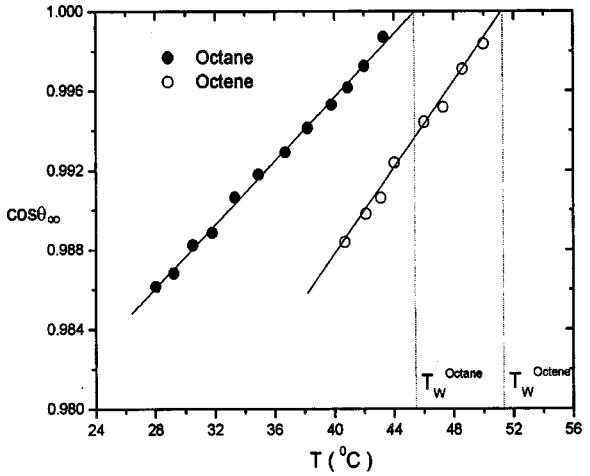

FIG. 7. Plot of $\cos\theta_\infty$ as a function of temperature T for *n*-octane and 1-octene. The solid lines are linear fits to the data while the wetting temperatures T_w corresponds to $\cos\theta_\infty=1$.

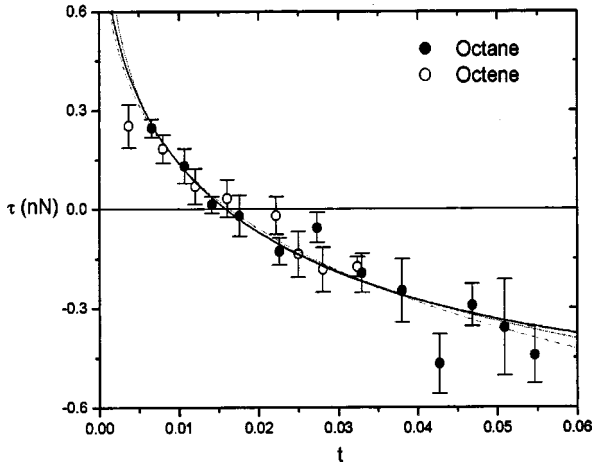

FIG. 8. Line tension τ as a function of the reduced temperature $t=(T_w-T)/T_w$ for *n*-octane and 1-octene. The solid, dashed, and dotted lines are fits to the octane data for short-ranged, nonretarded long-ranged, and retarded long-ranged interactions, respectively, using Eq. (14). If the octane data is fitted with the nonretarded interface potential model described by Eq. (13), this model gives a curve identical to the dashed line where $W_0=0.0018$ and $B\sigma_{lv}l_0=8.3\times10^{-9}$ N.

sensitive to the value of the liquid surface tension σ_{lv}; although both liquids have very close surface tension values ($\Delta\sigma_{lv}\simeq0.14$ mN/m) their wetting transition temperatures differ by nearly 6 °C. We have also measured the critical surface tension and wetting transition temperature for octane droplets on the same wafer but at different positions, or on different wafers but under the same silane preparation conditions. We find that the variabilities are less than 1 °C for T_w and 0.1 mN/m for σ_c. Such small variabilities in T_w and σ_c indicate that the SAMs exhibit excellent reproducibility and a low surface heterogeneity of $\Delta\sigma_c/\sigma_c\approx0.005$.

In Fig. 8 we plot the line tension τ as a function of the reduced temperature $t\equiv(T_w-T)/T_w$ for octane (solid circles) and octene (open circles). Both liquids exhibit almost identical behavior. This behavior agrees with many of the predictions in [53] and [61], specifically, for increasing temperatures towards T_w, τ changes from a negative to a positive value with an increasing absolute slope $|d\tau/dT|$. We have also used Eq. (14) to fit the octane data for short-ranged (solid line), nonretarded long-ranged (dashed line), and retarded long-ranged (dotted line) interactions where the adjustable parameters τ_0 and τ_1 are listed in Table III. From Fig. 8 one can readily see that the experimental resolution for τ and the range for ΔT are insufficient to distinguish be-

TABLE III. The values of τ_0 and τ_1 for different interactions in Eq. (14).

X	τ_0(nN)	τ_1(nN)
Short range	1.177	2.254
Nonretarded long range	−1.226	0.296
Retarded long range	1.754	3.482

tween the various models for short-range, nonretarded and retarded long-range interactions; these three interactions provide an equally good description of the experimental data. An unfortunate aspect of this method of analysis is that the physical meaning of the parameters τ_0 and τ_1, for each potential, is not at all clear and therefore it is difficult to assess whether the values obtained for these parameters are reasonable.

An alternative approach is to return to the more fundamental equation, Eq. (11), which relates the interaction potential $V(l)$ to the line tension τ. According to this approach the behavior exhibited in Fig. 8 is in qualitative agreement with the expectations of Eqs. (11) and (12) as the spreading coefficient $S \rightarrow 0$. At T_w the line tension τ is positive, as is observed, because for first-order wetting transitions the energy barrier which exists between the two minima at l_1 and $l=\infty$ gives rise to a positive area J_1 (while $J_2=0$ at T_w). The order of magnitude measured for $|\tau| \sim 10^{-10}$ N is in agreement within the upper limits expected from theory; however, upon closer inspection there are also significant quantitative differences between these experimental results and the theoretical calculations. Various models for the interaction potential $V(l)$ [14,50,61] determined that the line tension changes sign at a large contact angle $\theta_\infty \sim 60°$ or correspondingly at low temperatures $\Delta T = T_w - T \sim 30\,°\mathrm{C}$ well below T_w. In contrast the experiments for both liquids find that τ changes sign close to T_w at $t=0.016$ ($\Delta T \sim 5\,°\mathrm{C}$) corresponding to $\theta_\infty(\tau=0)=5.0°$. The experimental quantity $\theta_\infty(\tau=0)=5.0°$ provides important *microscopic* information about the shape of $V(l)$ because this quantity is determined by the integral in Eq. (11), independent of the magnitude of $B\sigma_{lv}l_0$, and occurs when the areas $J_1=J_2$ in Fig. 2(b).

What does the quantity $\theta_\infty(\tau=0)=5.0°$ tell us about the shape of $V(l)$? In order to examine this question we consider the phenomenological potential given in Eq. (13) which, as discussed previously, includes many physically reasonable features expected for a potential near a first-order wetting transition. For a given liquid-solid combination the Hamaker constant W and liquid-vapor surface tension σ_{lv} are known while the temperature variation of the spreading coefficient S can be deduced from Eq. (6) and Fig. 7. Hence in Eqs. (11) and (13) there are only two unknowns, namely, the position of the repulsive barrier l_0 and the scale factor B. [Recall that l_0 also determines the height of the repulsive barrier according to Eq. (13)]. These two parameters can be determined independently: l_0 determines when the integral in Eq. (13) is zero [corresponding to $\theta_\infty(\tau=0)=5.0°$] while B determines the absolute magnitude of the line tension τ. Hence $W_0 = W/\sigma_{lv}l_0^2 (=0.0018)$ was adjusted to provide agreement with the experimental condition that $\theta_\infty(\tau=0)=5.0°$ while the quantity $B\sigma_{lv}l_0 (=8.3\times10^{-9}$ N) was adjusted to provide the correct magnitude for τ. The results for τ as a function of t agree with the dashed line in Fig. 8, obtained previously using Eq. (14) for NLR interaction. The phenomenological potential [Eq. (13)] therefore provides a good description of the experiments. Both octane and octene possess a $W \approx 1.0 \times 10^{-21}$ J [76] and $\sigma_{lv} \approx 20.7$ mN/m. We therefore find that $l_0=(5.1\pm0.2)$ nm and $B=78\pm6$. The position of the repulsive barrier at $l_0=5.1$ nm is in reasonable agreement with the repulsive barrier measured for liquids between two mica plates in the surface forces apparatus of Israelachvili [77]. The scale factor $B=78$ determines the magnitude of the line tension τ.

Our line tension results are of similar magnitude ($|\tau| \approx 10^{-10}$ N) to a number of other groups [35,78] and are amongst the smallest values for liquid droplets situated on flat solid surfaces. In particular they agree in magnitude with the line tension measurements of Pompe, Fery, and Herminghaus [78] for droplets of hexaethylene glycol on rather similar surfaces. In this work the line tension was determined by examining the contact angle θ as a function of the *local* radius of curvature r (~ 0.1 to ~ 1 μm) for droplets deposited upon a structured Si wafer consisting of alternating hydrophilic (SiO_2) and hydrophobic (perfluorinated alkylsilane) stripes where the periodicity was of order 500 nm. The technique of tapping mode atomic force microscopy was used in this study of liquid droplets at very small length scales [79]. Line tension values of $|\tau| \approx 10^{-10}$ N for liquid droplets deposited upon Si wafers are approximately two orders of magnitude larger than values that are typically measured for liquid droplets on liquid surfaces [22,23,80]. This is perhaps not so surprising. It is well known that the surface energy of solid surfaces is frequently much larger than the surface tension of liquid surfaces, hence, droplets deposited upon a solid surface may well have a larger line tension than droplets deposited upon a liquid surface. There are additional complications for droplets deposited upon solid surfaces that are not present for droplets on liquid surfaces. For example, (i) solid surfaces possess a characteristic surface roughness [81–83] and (ii) molecularly smooth solid surfaces induce smectic layering within the first few monolayers of a liquid deposited upon such a surface [84]; it is not understood how either of these two effects influence the line tension. What we find so surprising and unexpected from this study is that Eqs. (11) and (13) can describe the experimental line tension results with a *constant* value of the scale factor B. These equations are expected to describe the line tension variation with temperature for liquid droplets on liquid surfaces with $B=1$. It is truly remarkable that these equations can continue to describe the line tension variation for droplets on solid surfaces for a constant $B \approx 100$ despite the additional complications which occur at solid surfaces. This implies that the integral within Eq. (11) correctly incorporates the required thermal dependence of the line tension.

V. SUMMARY

In this paper a microscopic interferometry technique was used to investigate the behavior of the line tension in the vicinity of a first-order wetting transition for *n*-octane or 1-octene droplets on a hexadecyltrichlorosilane coated Si wafer surface. The experimental results are in qualitative agreement with the interface displacement model of Indekeu and theoretical calculations of others which predict that the line tension should change from a negative to a positive value with increasing (negative) slope as the wetting transi-

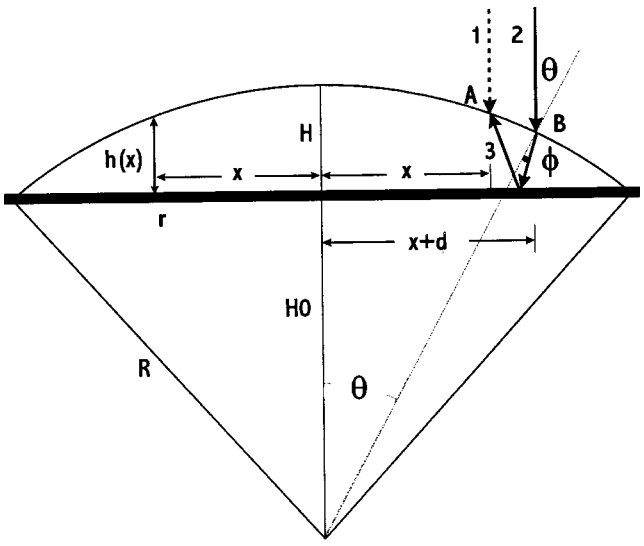

FIG. 9. Sketch of a spherical capped shaped droplet resting on a solid surface. The interference fringe at point *A* is formed by the illuminating beam 1 and the reflected beam 3 (which originates from illuminating beam 2 at point *B*).

tion temperature T_w is approached. The change in sign of τ with increasing temperature and the positive value of τ at T_w is a direct consequence of the presence of a repulsive barrier in the interface potential $V(l)$ for a first-order wetting transition. Our measurements cannot yet distinguish whether the short-range or long-range interactions make the dominant contribution to the line tension; however, a simple phenomenological model [Eqs. (11) and (13)] which possesses many realistic features correctly accounts for the experimental results with $l_0=5.1\pm0.2$ nm [corresponding to the position of the repulsive barrier in the interface potential $V(l)$] and $B=78\pm6$ (a scale factor which determines the magnitude of the line tension τ).

ACKNOWLEDGMENTS

Acknowledgment is made to the Donors of the Petroleum Research Fund, administered by the American Chemical Society, and to the National Science Foundation through Grant No. DMR-9631133 for partial support of this research.

APPENDIX

For a spherical droplet resting on a solid surface as sketched in Fig. 9, the shape of a droplet is described by

$$\begin{aligned} h(x) &= \sqrt{R^2-x^2}-H_0 \\ &\approx R\left(1-\frac{x^2}{2R^2}\right)-H_0 \quad (R\gg x) \\ &= H_0+H-\frac{x^2}{2R}-H_0 \\ &= H\left(1-\frac{x^2}{2RH}\right) \\ &\approx H\left(1-\frac{x^2}{r^2}\right) \quad (R\gg H), \end{aligned} \tag{A1}$$

and the contact angle θ is determined by

$$\tan\theta=\left|\frac{dh(x)}{dx}\right|_{x=r}=\frac{2H}{r}, \tag{A2}$$

which is used to calculate the contact angle in this paper. The contact angle may also be determined from the average value θ_{ave} of each fringe's contact angle θ_i calculated by

$$\tan\theta_i=\frac{2rh_i}{r^2-r_i^2-h_i^2}, \tag{A3}$$

where h_i and r_i correspond to the thickness and radius of the ith fringe of the droplet. To obtain the fitting parameters H and r, the value of h_i can be calculated from Eq. (16), an approximate interference condition, by assuming the refracted beam is perpendicular to the silicon wafer. To ensure that Eq. (16) is a good approximation, a strict interference condition is considered below.

The ith interference fringe at point A is formed from the interference between the illuminating beam 1 and the reflected beam 3 (originating from illuminating beam 2 at point B) as shown in Fig. 9. The distance between the two illuminating beams (1 and 2) is d. Then the strict interference condition is

$$h(x)-h(x+d)+n\sqrt{d^2+[h(x)+h(x+d)]^2}=i\lambda, \tag{A4}$$

where $h(x)$ is expressed as Eq. (A1) and

$$\begin{aligned} d &= \tan(\theta-\phi)[h(x)+h(x+d)] \\ &\approx [-h'(x+d)+h'(x+d)/n][h(x)+h(x+d)] \\ &= -h'(x+d)[h(x)+h(x+d)](1-1/n). \end{aligned} \tag{A5}$$

As an example, consider the interference fringes of octane at 40.9 °C shown in Fig. 4. The positions of the destructive and constructive interference fringes are determined by a computer program and displayed as square points in Fig. 4 (bottom graph). The droplet shape is fitted to Eq. (A1) (solid line) where the fitting parameters r and H are, respectively, 35.13 ± 0.03 μm and 1.568 ± 0.003 μm. The contact angle is therefore $\theta=5.099°\pm0.006°$ according to Eq. (A2). The contact angle may also be calculated from Eq. (A3) or by solving Eqs. (A1), (A4), and (A5) to give $\theta_{ave}=5.089°\pm0.006°$ or $\theta_{acc}=5.097°\pm0.006°$, respectively. These three contact angle determinations are the same within the calculated error. Hence the method that we used in this paper, Eqs. (15)–(17), is reliable for measuring small contact angles with a precision of better than 0.01°.

[1] M.V. Berry, J. Phys. A **7**, 231 (1974).
[2] B.A. Pethica, J. Colloid Interface Sci. **62**, 567 (1977).
[3] G. Navascués and P. Tarazona, J. Chem. Phys. **75**, 2441 (1981).
[4] G. Navascués and L. Mederos, J. Chem. Phys. **79**, 2006 (1983).
[5] J.A. de Feijter and A. Vrij, J. Electroanal. Chem. Interfacial Electrochem. **37**, 9 (1972).
[6] N.V. Churaev, V.M. Starov, and B.V. Derjaguin, J. Colloid Interface Sci. **89**, 16 (1982).
[7] J. S. Rowlinson and B. Widom, *Molecular Theory Capillarity* (Oxford Science, New York, 1984), p. 240.
[8] B.V. Toshev, D. Platikanov, and A. Scheludko, Langmuir **4**, 489 (1988).
[9] C. Varea and A. Robledo, Phys. Rev. A **45**, 2645 (1992).
[10] C. Varea and A. Robledo, Physica A **183**, 12 (1992).
[11] B.V. Toshev and M.Z. Avramov, Colloids Surf., A **100**, 203 (1995).
[12] W. Koch, S. Dietrich, and M. Napiorkowki, Phys. Rev. E **51**, 3300 (1995).
[13] T. Getta and S. Dietrich, Phys. Rev. E **57**, 655 (1998).
[14] H. Dobbs, Langmuir **15**, 2586 (1999).
[15] H. J. Schultze, *Physico-Chemical Processes in Flotation* (Elsevier, Oxford, 1984), p. 163.
[16] J. Mingins and A. Scheludko, J. Chem. Soc., Faraday Trans. 1 **75**, 1 (1979).
[17] Z. Zorin, D. Platikanov, and T. Kolarov, Colloids Surface **22**, 147 (1987).
[18] J.A. Wallace and S. Schurch, J. Colloid Interface Sci. **124**, 452 (1988).
[19] J.A. Wallace and S. Schurch, Colloids Surface **43**, 207 (1990).
[20] H. Vinke, G. Bierman, P.J. Hamerama, and J.M.H. Fortuin, Chem. Eng. Sci. **46**, 2497 (1991).
[21] R. Aveyard and J.H. Clint, J. Chem. Soc., Faraday Trans. **91**, 175 (1995).
[22] A. Dussaud and M. Vignes-Adler, Langmuir **13**, 581 (1997).
[23] R. Aveyard, J.H. Clint, D. Nees, and V. Paunov, Colloids Surf., A **146**, 95 (1999).
[24] J. Drelich and J.D. Miller, J. Colloid Interface Sci. **164**, 252 (1994).
[25] J. Drelich and J.D. Miller, Part. Sci. Technol. **10**, 1 (1992).
[26] J. Drelich, J.D. Miller, and J. Hupka, J. Colloid Interface Sci. **155**, 379 (1993).
[27] J. Gaydos and A.W. Neumann, J. Colloid Interface Sci. **120**, 76 (1987).
[28] L. Boruvka, J. Gaydos, and A.W. Neumann, Colloids Surface **43**, 307 (1990).
[29] D. Li and A.W. Neumann, Colloids Surface **43**, 195 (1990).
[30] D. Li, P. Cheng, and A.W. Neumann, Adv. Colloid Interface Sci. **39**, 347 (1992).
[31] D. Li, Colloids Surf., A **116**, 1 (1996).
[32] P. Chen, S.S. Susnar, A. Amirfazli, C. Mak, and A.W. Neumann, Langmuir **13**, 3035 (1997).
[33] R. Vera-Graziano, S. Muhl, and F. Rivera-Torres, J. Colloid Interface Sci. **170**, 591 (1995).
[34] *The Collected Works of J. Willard Gibbs* (Yale University Press, London, 1957), p. 288.
[35] J. Drelich, Colloids Surf., A **116**, 43 (1996).
[36] B.M. Law, Phys. Rev. Lett. **72**, 1698 (1994).
[37] M. Lazaridis, J. Colloid Interface Sci. **155**, 386 (1993).
[38] A.D. Alexandrov, B.V. Toshev, and A.D. Scheludko, Langmuir **7**, 3211 (1991).
[39] P.G. de Gennes, Rev. Mod. Phys. **57**, 827 (1985).
[40] E.B. Dussan, Annu. Rev. Fluid Mech. **11**, 371 (1979).
[41] I.B. Ivanov, P.A. Kralchevsky, and A.D. Nikolov, J. Colloid Interface Sci. **112**, 97 (1986).
[42] V.J. Novotny and A. Marmur, J. Colloid Interface Sci. **142**, 355 (1991).
[43] B.V. Toshev and D. Platikanov, Adv. Colloid Interface Sci. **40**, 157 (1992).
[44] I.B. Ivanov, P.A. Kralchevsky, A.S. Dimmitrov, and A.D. Nikolov, Adv. Colloid Interface Sci. **39**, 77 (1992).
[45] I.B. Ivanov, A.S. Dimmitrov, A.D. Nikolov, N.D. Denkov, and P.A. Kralchevsky, J. Colloid Interface Sci. **151**, 446 (1992).
[46] A.S. Dimmitrov, A.D. Nikolov, N.D. Denkov, P.A. Kralchevsky, and I.B. Ivanov, J. Colloid Interface Sci. **151**, 462 (1992).
[47] J.F. Joanny and P.G. de Gennes, J. Colloid Interface Sci. **111**, 94 (1986).
[48] B. Widom and A.S. Clarke, Physica A **168**, 149 (1990).
[49] B. Widom and H. Widom, Physica A **173**, 72 (1991).
[50] J.O. Indekeu, Physica A **183**, 439 (1992).
[51] J.O. Indekeu, G. Backx, and G. Langie, Physica A **196**, 335 (1993).
[52] J.O. Indekeu and A. Robledo, Phys. Rev. E **47**, 4607 (1993).
[53] J.O. Indekeu, Int. J. Mod. Phys. B **8**, 309 (1994).
[54] A. Robledo, C. Varea, and J.O. Indekeu, Phys. Rev. A **45**, 2423 (1992).
[55] H.T. Dobbs and J.O. Indekeu, Physica A **201**, 457 (1993).
[56] A. Robledo and J.O. Indekeu, Europhys. Lett. **25**, 17 (1994).
[57] M. Schick and P. Taborek, Phys. Rev. B **46**, 7312 (1992).
[58] D.B. Abraham, F. Latrémolière, and P.J. Upton, Phys. Rev. Lett. **71**, 404 (1993).
[59] B. Widom, J. Phys. Chem. **99**, 2803 (1995).
[60] B. Widom, in *Condensed Matter Theories*, edited by L. Blum and F. B. Malik (Plenum, New York, 1993), Vol. 8, p. 589.
[61] I. Szleifer and B. Widom, Mol. Phys. **75**, 925 (1992).
[62] E.M. Blokhuis, Physica A **202**, 402 (1994).
[63] C. Bauer and S. Dietrich, Eur. Phys. J. B **10**, 767 (1999).
[64] S. Perković, E.M. Blokhuis, E. Tessler, and B. Widom, J. Chem. Phys. **102**, 7584 (1995).
[65] S. Perković, E.M. Blokhuis, and G. Han, J. Chem. Phys. **102**, 400 (1995).
[66] J.Y. Wang, S. Betelu, and B.M. Law, Phys. Rev. Lett. **83**, 3677 (2000).
[67] A.I. Rusanov, Surf. Sci. Rep. **23**, 173 (1996).
[68] F. Brochard-Wyart, Langmuir **7**, 335 (1991).
[69] S. Dietrich, in *Phase Transitions and Critical Phenomena*, edited by C. Domb and J.L. Lebowitz (Academic, London, 1988), Vol. 12, p. 1.
[70] J.W. Schmidt and M.R. Moldover, J. Chem. Phys. **79**, 379 (1983).
[71] K. Ragil, J. Meunier, D. Broseta, J.O. Indekeu, and D. Bonn, Phys. Rev. Lett. **77**, 1532 (1996).
[72] W.A. Zisman, Adv. Chem. Ser. **43**, 1 (1964).
[73] S.R. Wasserman, Y.T. Tao, and G.M. Whitesides, Langmuir **5**, 1074 (1989).
[74] J.B. Brzoska, I. Ben Azouz, and F. Rondelez, Langmuir **10**, 4367 (1994).

[75] J.J. Jasper, J. Phys. Chem. Ref. Data **1**, 891 (1972).
[76] V.A. Parsegian and B.W. Ninham, J. Theor. Biol. **38**, 101 (1973).
[77] J. N. Israelachvili, *Intermolecular and Surface Forces* (Academic, London, 1992), 2nd ed.
[78] T. Pompe, A. Fery, and S. Herminghaus, J. Adhes. Sci. Technol. **13**, 1155 (1999); T. Pompe and S. Herminghaus, Phys. Rev. Lett. **85**, 1930 (2000).
[79] S. Herminghaus, A. Fery, and D. Reim, Ultramicroscopy **69**, 211 (1997).
[80] D. Bonn, E. Bertrand, J. Meunier, and R. Blossey, Phys. Rev. Lett. **84**, 4661 (2000).
[81] M.O. Robbins and J.F. Joanny, Europhys. Lett. **3**, 729 (1987).
[82] E.L. Decker and S. Garoff, J. Adhes. **63**, 159 (1997).
[83] In [66] we assumed that the large value for the scale factor B was due to the presence of surface roughness on the solid surface.
[84] A.A. Chernov and L.V. Mikheev, Phys. Rev. Lett. **60**, 2488 (1988).